Infrared Physics & Technology 77 (2016) 382–390

Contents lists available at ScienceDirect

Infrared Physics & Technology

journal homepage: www.elsevier.com/locate/infrared

Regular article

Infrared imaging based hyperventilation monitoring through respiration rate estimation

Anushree Basu [a,*], Aurobinda Routray [a], Rashmi Mukherjee [a], Suprosanna Shit [b]

[a] Department of Electrical Engineering, Indian Institute of Technology Kharagpur, West Bengal, India
[b] Department of Electrical Engineering, Jadavpur Uiversity, West Bengal, India

HIGHLIGHTS

- Infrared thermography based hyperventilation detection has been considered.
- Minimum eigenvalue features are taken as tracking features.
- Motion tracking has been done using Kanade–Lucas–Tomasi algorithm.
- Respiration rate estimation using spirometer test has been done for validation.
- Qualitative comparative analysis between previous literature and proposed method.

ARTICLE INFO

Article history:
Received 4 September 2015
Revised 12 June 2016
Accepted 14 June 2016
Available online 15 June 2016

Keywords:
Hyperventilation
Minimum eigenvalue
ROI selection
Thresholding
Respiration rate
Thermography

ABSTRACT

A change in the skin temperature is used as an indicator of physical illness which can be detected through infrared thermography. Thermograms or thermal images can be used as an effective diagnostic tool for monitoring and diagnosis of various diseases. This paper describes an infrared thermography based approach for detecting hyperventilation caused due to stress and anxiety in human beings by computing their respiration rates. The work employs computer vision techniques for tracking the region of interest from thermal video to compute the breath rate. Experiments have been performed on 30 subjects. Corner feature extraction using Minimum Eigenvalue (Shi–Tomasi) algorithm and registration using Kanade Lucas–Tomasi algorithm has been used here. Thermal signature around the extracted region is detected and subsequently filtered through a band pass filter to compute the respiration profile of an individual. If the respiration profile shows unusual pattern and exceeds the threshold we conclude that the person is stressed and tending to hyperventilate. Results obtained are compared with standard contact based methods which have shown significant correlations. It is envisaged that the thermal image based approach not only will help in detecting hyperventilation but can assist in regular stress monitoring as it is non-invasive method.

1. Introduction

In recent times, the advent of infrared thermography (IRT) has ushered in a new direction towards non-invasive diagnosis of various diseases, taking into account the fact that there is a change in the skin temperature leading to abnormal thermal patterns due to pathological conditions [1]. Various clinical applications of IRT in medical field include diabetic neuropathy, breast cancer detection, fever screening, vascular disorder, rheumatologic diseases, gynecological problems, dermatological conditions, brain imaging, etc. which have been studied by several researchers [2]. One of the important applications of IRT is the monitoring of the vital signs i.e. body temperature, blood pressure, heart rate and respiration rate. The recording of the vital signs becomes crucial for assessing the physical health condition of a person since abnormal variations in these parameters may cause severe illness. Abnormalities in body temperature may be due to fever, infection, stress, dehydration, etc. Serious health issues like atherosclerosis, heart failure, stroke, and hyper tension may result due to high blood pressure. Pulse rate which denotes the number of times heart beats per minute is another important parameter which needs to be in control as its increase indicates stress, anxiety, thyroid disorder, shock, anemia, etc. Finally, a proper check on respiration rate (RR) i.e. number of breaths per minute is necessary to keep a check on breathing problems like asthma, hyper or hypo-ventilation, respiratory alkalosis, apnea, anxiety, pneumonia, congestive heart failure, lung disease, use of narcotics, or drug overdose. This work

* Corresponding author.
E-mail address: ele.anushree09@gmail.com (A. Basu).

http://dx.doi.org/10.1016/j.infrared.2016.06.014
1350-4495/

proposes a non-contact and non-invasive indication of hyperventilation by estimating the RR through IRT. The term hyperventilation refers to the specific clinical condition where breathing becomes rapid or fast leading to an unbalance between the inhaled oxygen (O_2) and exhaled carbon dioxide (CO_2) thus giving way to respiratory alkalosis [3]. It results in more exhalation than inhalation causing reduction in the level of carbon dioxide in blood. As such, blood vessels supplying blood to the brain system gets constricted. There is a reduced blood supply which causes lightheadedness, dizziness, muscle spasm, weakness, etc. Hyperventilation is a symptom caused due to anxiety, panic, stress, nervousness, etc. This condition is generally diagnosed by regular monitoring of the breathing rate of a person [4] and its pH level. Hence, RR becomes very vital in such kind of critical conditions. In recent times monitoring of RR has also been applied in polygraph testing; sleep studies, patient monitoring, etc. [5].

1.1. Respiration rate and thermography

RR may be defined as the number of complete respiration cycles in a minute. The respiration cycle of a human being can be divided into the three following stages [6]:

- Inspiration stage: Breathing air in.
- Expiration stage: Breathing air out.
- Post-expiration stage: Equalization of pressure in the lungs and atmosphere.

The time period for respiration is the time interval between the start of the inspiration stage and the end of the post-expiration stage. During rest condition average RR of an adult ranges from 12 to 20 breaths/min. RR may also increase due to fever or other medical conditions [7]. For a person undergoing physical exertion, RR increases in the range up to 35–40 breaths/min [5]. If this rate increases beyond 40, the person is said to have hyperventilation syndrome [8]. In general hyperventilation is a condition of a person when his/her breathing rate becomes much higher than the normal rate without undergoing any kind of physical exhaustion. As such, it is absolutely necessary to monitor the RR; else hyperventilation may lead to serious health hazards viz. respiratory alkalosis, carpopedal spasms, etc. [9]. Thermography or thermal imaging captures the thermal radiation emitted from an object using an infrared imaging sensor. This is further converted to pseudo colored thermal images also known as thermograms [10]. The infrared radiations consist of three spectral regions [11]:

1. Shortwave (SW): 0.9–1.7 μm.
2. Midwave (MW): 3–5 μm.
3. Longwave (LW): 7–14 μm.

Thermal imaging gives a map of the heat distribution of an image from which we can get information on the hot spots. During inhalation the air goes inside the nasal cavity and passes down to the lungs through the nasopharynx, larynx and trachea and vice versa during exhalation [12]. Fig. 1 depicts the human respiratory pathway. During exhalation nostril is warmer as compared to that of inhalation. The temperature around the nostrils is tracked continuously for one minute which gives a quasi-periodic thermal pattern where rise and fall of temperature corresponds to exhalation and inhalation respectively [13]. This profile thus gives an estimation of the respiration rate and the breath pattern.

1.2. Background

Hyperventilation syndrome is closely related with anxiety disorders and panic. During panic attack many individuals tend to hyperventilate resulting in respiratory alkalosis which may lead to serious diseases. To study the effect of hyperventilation researchers generally use the method of voluntary hyperventilation where the individuals are asked to breath in a particular fashion [14]. Voluntary hyperventilation causes an increase in the RR along with a decrease in the pCO_2 i.e. partial pressure of arterial blood carbon dioxide [15]. It also results in hypocapnic state in which there is a decrease in the cerebral blood flow (CBF), increase in cerebral oxygen consumption and decrease in cardiac output [16,17]. This work mainly focuses on RR computing and monitoring the breath pattern during voluntary hyperventilation using thermographic videos. Different contact-based measurement methods for RR estimation of an individual are in practice. Moody et al. [18] developed a method of RR measurement using Electrocardiogram (ECG) electrodes and sensors based on the phenomena of sinus arrhythmia. This method was further amended by the implementation of the BioMatt method [19], which did not use any electrodes to measure breathing and cardiac activity. However, it failed to distinguish motion due to breathing and body movement. This was rectified by Larson et al. by the use of signal processing technique which separated out the components of BioMatt signal [20]. Similarly other methods were developed for measuring RR which includes measurement of changes in blood volume [21], changes occurring to thoracic or abdominal circumference, etc. [22]. However, being contact based methods, these technique cause discomfort to individuals. Non contact method of RR estimation started through Radar Vital Signs Monitor [23] which could measure RR from a distance of up to 15 feet behind an 8 in. hollow concrete or wooden wall. This method has a limitation since motion artefacts distort breath signals. Infrared imaging technique is first employed by Pavlidis et al. [24] to compute RR. Chekmenev et al. [25] also suggested measurement of heart rate as well as RR through thermography. RR computations in a non-contact manner from thermal images using algorithms such as Fast Fourier Transform and statics based methods have also been proposed [26,27]. Fast Fourier analysis and adaptive filtering technique has been employed for the measurement of contact free cardiac pulse rate analysis [28]. Moreover, thermal infrared imaging has also been used for diagnosis of sleep apnea, hypopnea, etc. by airflow monitoring during polysomnography [29]. The main challenge of RR computation based on IRT is proper tracking of the region of interest (ROI) which is responsible for giving appropriate thermal signature corresponding to the breath pattern. Khalidi et al. performed a nose segmentation procedure which divided the nose region into eight concentric segments and the thermal signature along all of them were tracked [30]. Matsui et al. proposed a non-contact based method for screening patient having infection, which accumulates respiration rate using microwave radar, skin temperature by thermography and classification is done

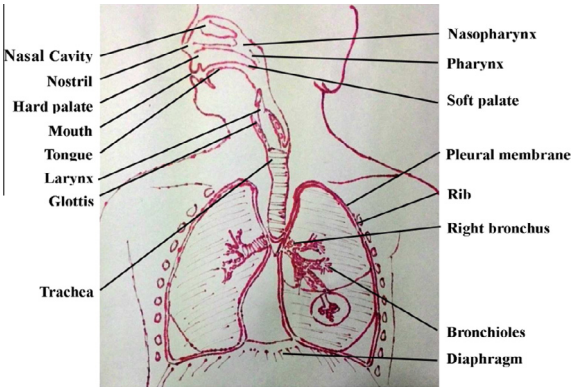

Fig. 1. Respiratory system of human being.

using linear discriminant function [31]. Abbas et al. attempts to detect RR of neonates on a real time basis using IRT but fixed ROI is assumed after initialization [32]. Lewis et al. [33] devised a method to extract RR and relative tidal volume by tracking nostril region of infrared video using Piecewise Bzier Volume Deformation model (PBVD) developed by Tao and Huang [34]. Nostril segmentation based on Chan–Vese active contour model framework has been adopted for tracking the spatiotemporal dynamic behavior of the thermal videos during the breathing mechanism [35]. A particle filter facial tracking algorithm using Bayesian formula was proposed by Eveland et al. Particle filter based trackers have been used in many cases for RR estimation as suggested in the previous literature [36,37], however; due to its technical complexity particle filtering becomes a time consuming procedure.

The present work aims at RR estimation and monitoring of breath pattern in a simplified way and consuming less amount of time. Extensive literature review shows no reports on detecting hyperventilation using thermography. Thus the objective of this work is to detect whether a person is healthy or hyperventilating in a non-contact way from the breath pattern by tracking the corner features extracted from the region of interest in the thermal video frames using the Shi–Tomasi corner detection and Kanade–Lucas Tomasi registration algorithms.

2. Material and methods

2.1. Methodology

The methodology proposed in this work consists of the following steps (Fig. 2):

1. Initializing the ROI (region of interest) by Bounding Box in the thermal image.
2. Automatic Corner Feature detection on this ROI.
3. Automatic Tracking/Registration of selected corner features.
4. Thermal Signature Mapping.
5. Low-pass Filtering.
6. Computation of the RR.
7. Classification.

2.1.1. Bounding box selection of ROI

It is established that the occurrence of hot-spot can be detected by monitoring the lower nose region rather than the whole human face. Previous reports suggest that the temperature near the nose and the ear lobes are lower than other facial parts due to lack of blood supply. Moreover, convection causes cooling effect in these regions as they are in more direct contact with ambient conditions [38]. Hence, nasal area is the most suitable region for tracking the breathing cycle. Initially, ROI was marked out manually around the lower nose region with a bounding box. Subsequently it was automatically tracked by a corner detection and registration process as discussed in the subsequent paragraphs. One of the existing technique to localize ROI around nostril is to locate two hotspot around two eyes and then find a comparatively cold nose tip with distance constraint but this method wont work if the subject wear spectacles or one of the eyes is not clearly visible which leads to wrong detection of ROI. Other method is to detect only the coolest region of human face which is also ambiguous because in some case cheeks are cooler than nose tip. Hence to get rid of initialization error problem manually a rectangular area is identified around nostril that we called Bounding Box.

2.1.2. Corner feature detection

The regions having large intensity variations in all directions in an image are considered as corners, which are good for tracking purposes. In case of thermal images the intensity of the pixels are directly correlated with temperatures. Thus the pixels, close to the nostrils, having higher intensity variations are those which are affected due to the change in the breathing phenomenon. Hence, the rise in the temperature near the nostril causes a considerable amount of variations in the pixel intensities, which can be chosen as the corner feature points and tracked for monitoring the breath pattern. This paper uses the Minimum Eigenvalue feature detection (Shi–Tomasi) methodology to do the same [39]. Although, several other features i.e. Binary Robust Invariant Scalable Keypoints (BRISK), Features from Accelerated Segment Test (FAST), Speeded Up Robust Features (SURF), Harris features, etc. can also be used for corner features detection but in this work it is established that Minimum Eigenvalue features are best suited for thermal images. The comparison is shown in the results and discussions section.

Harris–Stephens algorithm: The Shi–Tomasi method is derived from the Harris–Stephens corner detection [40]. The Harris corner detector is implemented by scanning an image through a window function and incrementally shifting it in various directions while

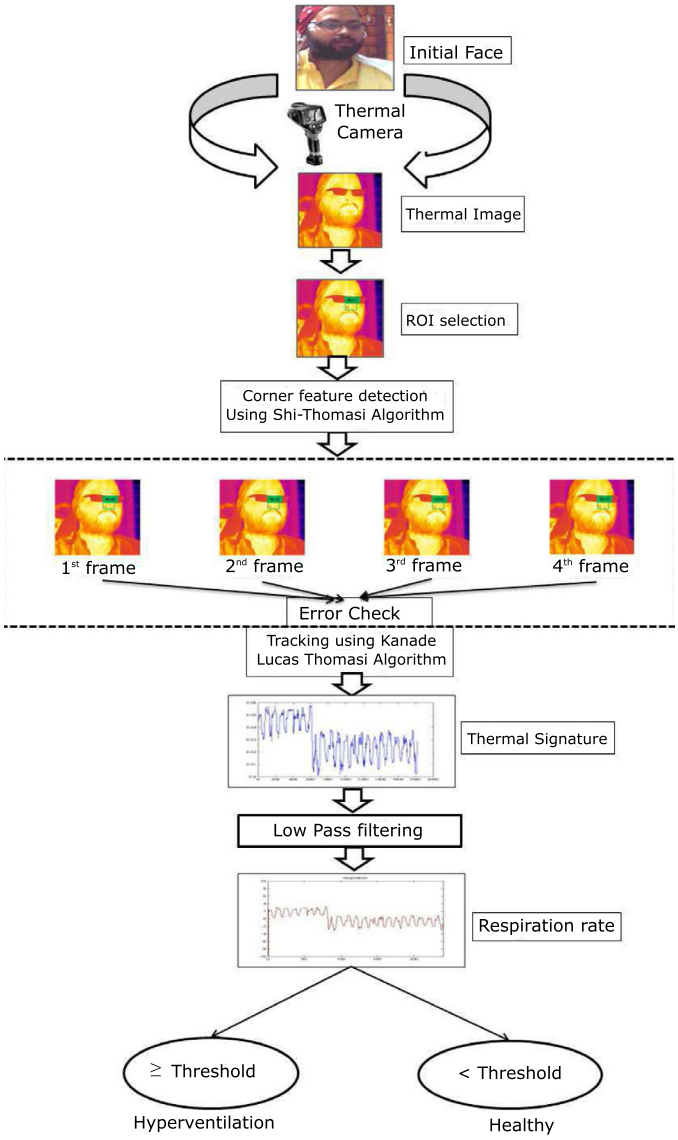

Fig. 2. Proposed workflow.

determining the average changes in image intensity. The corner detector operator can be given as:

$$E(p,q) = \sum_x \sum_y w(x,y)[I(x+p,y+q) - I(x,p)]^2 \quad (1)$$

where

E – Sum of squared differences between original and moved window,
p – Window displacement in x direction,
q – Window displacement in y direction,
$w(x,y)$ – Weighting function of the window,
$I(x+p,y+q)$ – Intensity of the moved window,
$I(x,y)$ – Intensity of the original window.

Simplifying the above expression using a Taylor series approximation of

$$I(x+p,y+q) - I(x,y) \approx I(x,y) + pI_x + qI_y - I(x,y) \quad (2)$$

we get

$$E(p,q) \approx \sum_x \sum_y w(x,y)[I(x,y) + pI_x + qI_y - I(x,y)]^2 \quad (3)$$

in matrix from:

$$E(p,q) \approx \sum_x \sum_y [p \quad q] w(x,y) \begin{bmatrix} I_x^2 & I_xI_y \\ I_yI_x & I_x^2 \end{bmatrix} \begin{bmatrix} p \\ q \end{bmatrix} \approx [p \quad q] M \begin{bmatrix} p \\ q \end{bmatrix} \quad (4)$$

where M is given as:

$$M = \sum_x \sum_y w(x,y) \begin{bmatrix} I_x^2 & I_xI_y \\ I_yI_x & I_x^2 \end{bmatrix} \quad (5)$$

Now, considering α and β as the eigenvalues of the matrix M, we define a parameter R such that

$$R = det(M) - k(trace(M))^2 \quad (6)$$

where $det(M) = \alpha\beta$,

$trace(M) = \alpha + \beta$,
R is considered to be in the corner region when it has a large positive value.

Shi–Tomasi Corner Detection Algorithm: [39] This algorithm is a modification of the above mentioned algorithm where the constant R is chosen as:

$$R = min(\alpha\beta) \quad (7)$$

where R is considered as a corner if its value is greater than a certain threshold.

2.1.3. Tracking/registration of selected features

Kanade–Lucas–Tomasi (KLT) method has been used here to register the images in the video-frames with respect to the corner points found by Shi–Tomasi technique [41]:

Kanade–Lucas–Tomasi (KLT) registration algorithm: It may be assumed that the adjacent video frames are related amongst themselves by a translational motion. The KLT algorithm tracks the incremental changes by comparing the parameter which minimizes the dissimilarity measured between the frames in the ROI. Considering $A(x)$ and $B(x)$ as two functions each giving respective pixel values at location x in two images. Let a parameter h (call it as disparity vector) exists which minimizes the difference measure between $A(x+h)$ and $B(x)$ for some x in a ROI C. Various measures of error such as L_1 or L_2 norm of the matrix and negative of normalized correlation can be used to find the difference. In this paper, L_2 norm of the difference in pixel values has been used. Thus the error measure can be written as (see Fig. 3):

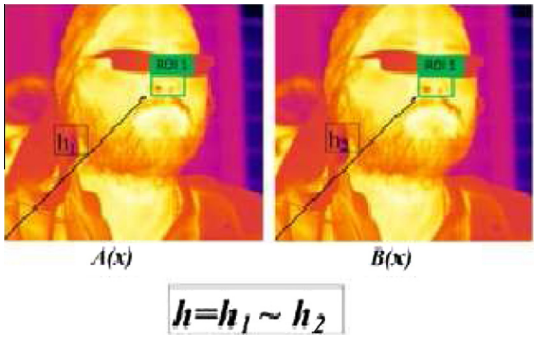

Fig. 3. Tracking window in two frames.

$$E = \sum_{x \in R} [A(\mathbf{x}+\mathbf{h}) - B(\mathbf{x})]^2 \quad (8)$$

where $\mathbf{x}$ and $\mathbf{h}$ are two dimensional row vectors in this case. Thus doing a linear approximation we get,

$$A(\mathbf{x}+\mathbf{h}) \approx A(\mathbf{x}) + \mathbf{h}\frac{\partial A(\mathbf{x})}{\partial \mathbf{x}} \quad (9)$$

where the column vector $\frac{\partial}{\partial \mathbf{x}}$ can also be represented as $\frac{\partial}{\partial \mathbf{x}} = \left[\frac{\partial}{\partial x_1} \quad \frac{\partial}{\partial x_2}\right]^T$ is the gradient operator with respect to $\mathbf{x}$. Thus minimizing the error we set the derivative of E with respect to $\mathbf{h}$ as zero.

$$\frac{\partial E}{\partial \mathbf{h}} = 0 \quad (10)$$

$$\frac{\partial}{\partial \mathbf{h}} \sum_{x \in R} \left[A(\mathbf{x}) + \mathbf{h}\frac{\partial A(\mathbf{x})}{\partial \mathbf{x}} - B(\mathbf{x})\right]^2 \approx 0 \quad (11)$$

$$\sum_{x \in R} 2\frac{\partial A}{\partial \mathbf{x}} \left[A(\mathbf{x}) + \mathbf{h}\frac{\partial A(\mathbf{x})}{\partial \mathbf{x}} - B(\mathbf{x})\right] = 0 \quad (12)$$

Simplifying the above equation we get,

$$\boldsymbol{h} \approx \left[\sum_{\mathbf{x}} \left(\frac{\partial A}{\partial \mathbf{x}}\right)^T [B(\mathbf{x}) - A(\mathbf{x})]\right] \left[\sum_{\mathbf{x}} \left(\frac{\partial A}{\partial \mathbf{x}}\right)^T \left(\frac{\partial A}{\partial \mathbf{x}}\right)^{-1}\right] \quad (13)$$

Although it is a continuous differential equation a numerical method based approach has been used for the solution. Thus having found the estimate of $\mathbf{h}$, Newton–Raphson iteration is used to find the sequence of estimates of $\mathbf{h}$ so that finally it converges to its best value. Taking,

$$\mathbf{h}_0 = 0$$

$$\mathbf{h}_{k+1} = \mathbf{h}_k + \left[\sum_{\mathbf{x}} w(\mathbf{x}) \left(\frac{\partial A}{\partial \mathbf{x}}\right)^T\right] \times \left[\sum_{\mathbf{x}} \left(\frac{\partial A}{\partial \mathbf{x}}\right)^T \left(\frac{\partial A}{\partial \mathbf{x}}\right)^{-1}\right] \quad (14)$$

here, the weighting function $w(\mathbf{x})$ can be defined as $A^2(\mathbf{x})$ or $\frac{\partial A^2}{\partial \mathbf{x}}$. The features of the selected region of interest of one frame are iteratively registered with the next frame by the above algorithm. This is again backtracked to the previous frame giving rise to a backward tracking error (Fig. 4). The total error due to forward and backward tracking is suitably thresholded to register the ROI in the next frame. The error threshold has been found by trial and error for the best results.

2.1.4. Thermal signature mapping

Thermal signature or profile is obtained from the ROI by tracking video frames using the above mentioned algorithms. The pixels of a thermal image are a representative of the temperatures at

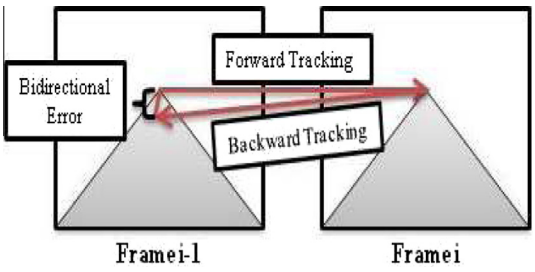

Fig. 4. Error thresholding.

Fig. 5. Experimental setup.

those points. Thus as the person inhales and exhales there is a change in the pixel intensity around the ROI. The corner features which are feature points having maximum variations in the intensity are thus tracked in all the frames on the basis of changing pixel intensities. The average pixel intensity of the ROIs of all frames is computed and taken as the reference value. As such, the raw thermal profile is obtained by checking the increase and decrease in the intensity values from the reference as the person inhaled or exhaled.

2.1.5. Low pass filtering

The thermal profile obtained from the chosen ROI may contain some amount of noise due to head or body movements and also noises due to atmospheric disturbances. Hence, the raw thermal profile is filtered using a low pass filter to obtain the breath pattern from which the RR was finally computed. Finite Impulse Response (FIR) low pass filter of order 32 and cut off frequency 5 Hz employing Kaiser Windowing method has been used in this work.

2.1.6. Computation of Respiration Rate (RR)

RR is computed from the low pass filtered signal by detecting number of peaks. The peaks present in the profile gives the number of exhalations while the crest gives the number of inhalations. One peak and one crest makes one complete breath cycle. Thus the total number of breath cycles in one minute gives the RR.

2.1.7. Classification

A simple methodology is proposed for classification in this paper. Classification of people based on their RR into two classes, i.e. healthy and hyperventilating is computed using a thresholding technique. Normal distributions for the two classes are fitted on the experimental data on the basis of maximum likelihood estimation technique. The point of intersection between the overlapping distributions is found out and the x co-ordinate corresponding to the intersection is chosen as the optimal thresholds.

The threshold is considered between class I (healthy) and class II (hyperventilating). A decision boundary is drawn on the basis of the threshold as shown in the results section. Thus a person having RR less than the threshold has been considered as a healthy individual under resting condition, while the person having RR more than the threshold has been considered as an hyperventilating individual (Fig. 14).

2.2. Experimental setup

A database of thermal images is created to test the performances of the algorithm. IRT experiments depend a lot on the environmental conditions such as humidity, airflow, and atmospheric temperature. Thus it is required to perform the experiments in a controlled atmosphere as the changes are within few degrees. Standard protocols are followed for performing experiments on thermography.

During the experiment the subjects are seated comfortably in a fixed chair in a temperature controlled room. The ambient room temperature is taken as 25 °C. The subjects are given 10 min duration to get acclimatized with the environment. Thirty subjects (age group 20–50 years; 18 males; 12 females) participated in the experiment after giving their informed consent. The participants are instructed not to have any kind of caffeine or medicines few hours before the experiment. Two types of IR image sequences of the face region are captured during this study:

A. *Natural breathing in resting condition*: Subjects are asked to breathe in and out normally for 5 min as their thermal videos are being captured. They are asked to keep the head region still as far as they can to reduce the effect of motion artifacts.
B. *Voluntary hyperventilation*: Subjects are asked to hyperventilate i.e. to breath in and out very fast continuously for 2 min through their nose. Their breathe rates are also similarly recorded using the thermal video camera.

Fig. 5 shows the schematic diagram of experimental setup. A video thermal camera with an uncooled microbolometer type detector operating in the range of 7.5–14 μm was used for the purpose. The Fluke Ti400 camera used has a focal plane array (FPA) with maximum resolution of 320 × 240 pixels and a maximum sampling rate of 60 fps. The sensitivity of the imager is less than 0.05 °C. Eight different types of standard as well as ultra-contrast color palettes are present to capture desired color platforms for analyzing the images. The data recorded from the imager are sent to MATLAB for analysis and classification using the algorithms stated earlier.

Spirometric test: The subjects are asked to relax for 15 min after performing the two sets of experiment as mentioned above. After completion of the resting phase the spirometer test, which is a contact based test, is conducted on all the subjects to compute their normal as well as hyperventilating RR. The normal RR of a person was obtained from the Slow Vital Capacity (SVC) test using a spirometer (Helios 40). The graph also indicates the respiration profile where the rising and falling edges of the volume curve denotes inhalation and exhalation phases respectively. Similarly, Maximum Ventilatory Volume (MVV) test taken for 1 min duration, can also give the respiration profile during hyperventilation. The Spirometer and the screen shots of the SVC plot are shown in Fig. 6.

3. Results and discussion

The step by step results obtained from the above experiment is shown in the following section. The suitability of the proposed

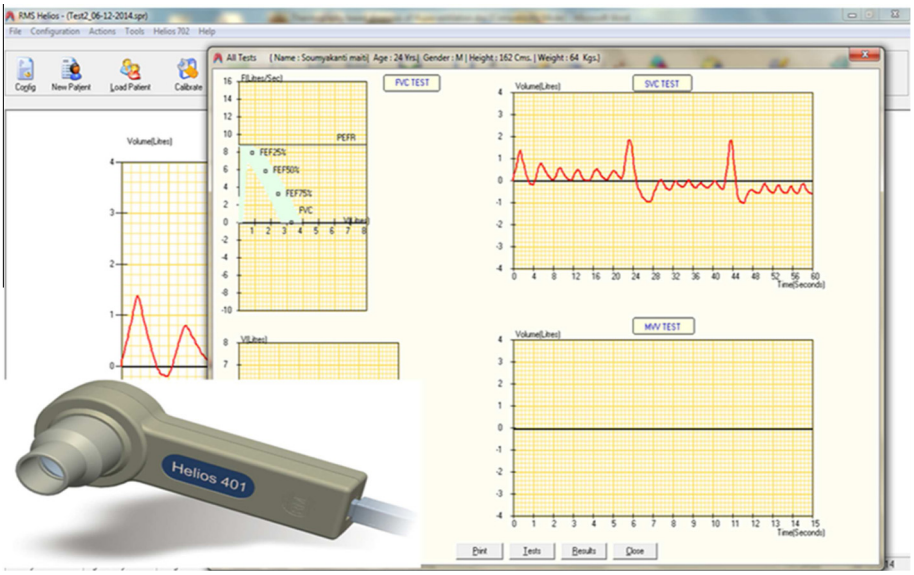

Fig. 6. Helios spirometer and corresponding software.

methodology as compared to some of the already reported studies is also discussed here. All the subjects are given sets of instructions before the data are recorded.

3.1. Normal breathing condition

The subjects are asked to sit, relax and breathe normally for 5 min. The video is recorded and the ROI is chosen accordingly from the recorded video. The selection of ROI is shown in Fig. 7. Corner features are detected using the algorithms like Harris detector, SURF features, FAST features, BRISK features as well as Minimum Eigenvalue features. The results are shown in Fig. 8. It is apparent from Fig. 8f that the Minimum Eigenvalue features are more prominent. It is suitable for thermal imaging techniques specifically when the ROI is very small. Thus the feature detection and its tracking is carried out by using the Shi–Tomasi and the KLT tracking algorithm. The thermal profile along the frames (averaged over the ROI of the respective frames) is shown in Fig. 9. This is further passed through the low pass filter (Fig. 10).

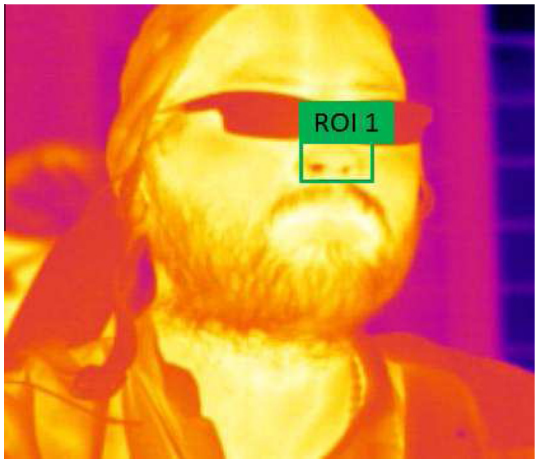

Fig. 7. ROI selection.

Fig. 8. Corner feature extraction using different algorithms.

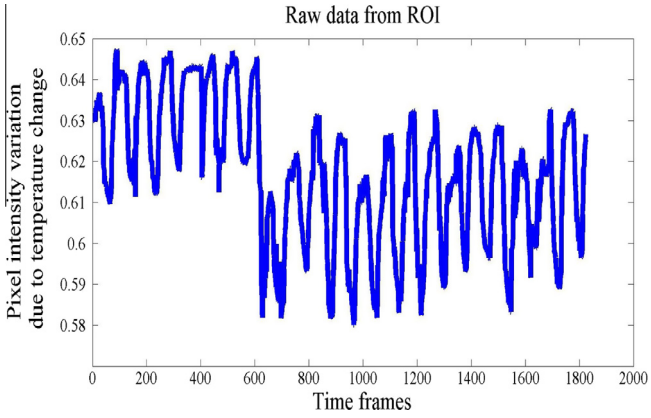

Fig. 9. Thermal profile obtained from ROI for normal breathing condition.

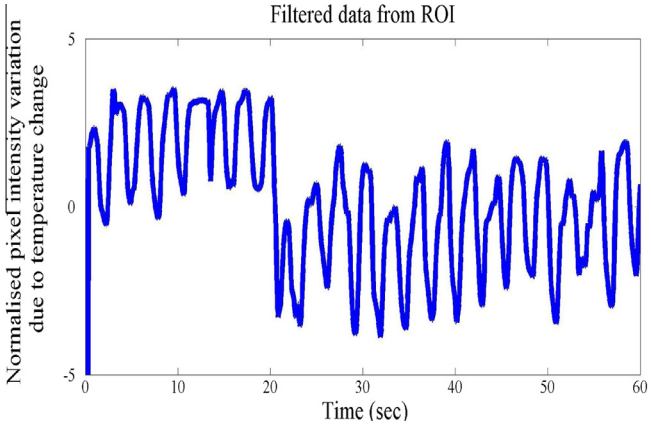

Fig. 10. Low pass filtered respiration profile obtained from the thermal profile for normal.

3.2. Breathing pattern while hyperventilating

The subjects are asked to perform voluntary hyperventilation for two mins. The thermal profile of one of these subjects is shown in the figure below (see Fig. 11). The subjects reported certain kind of dizziness, light headedness, etc. after this phase of experiment. This feeling gradually reduced during resting phase.

3.3. Classification

The data obtained from the 30 subjects during normal breathing and during hyperventilating conditions is given in Table 1 The data is classified using maximum likelihood estimation and the thresholding technique as earlier explained in Section 2. Fig. 12 shows that the threshold is at 23.99. Thus, the people having RR less than 24 are considered as normal healthy persons, the people having RR much above their normal level during resting condition are considered as hyperventilating.

Table 1
Table showing the breaths per minute for all 30 subjects during normal breathing, physical exercise and hyperventilation.

Sl. no.	Name	Breaths per minute	
		Normal breathing	Hyperventilating
1.	Sub 1	19	35
2.	Sub 2	22	38
3.	Sub 3	15	29
4.	Sub 4	18	41
5.	Sub 5	18	46
6.	Sub 6	16	38
7.	Sub 7	21	48
8.	Sub 8	19	40
9.	Sub 9	23	43
10.	Sub 10	14	22
11.	Sub 11	18	39
12.	Sub 12	17	42
13.	Sub 13	20	45
14.	Sub 14	13	20
15.	Sub 15	19	45
16.	Sub 16	17	37
17.	Sub 17	22	43
18.	Sub 18	16	28
19.	Sub 19	19	36
20.	Sub 20	18	39
21.	Sub 21	20	41
22.	Sub 22	16	29
23.	Sub 23	14	21
24.	Sub 24	18	44
25.	Sub 25	18	37
26.	Sub 26	23	35
27.	Sub 27	15	23
28.	Sub 28	17	38
29.	Sub 29	21	47
30.	Sub 30	19	38

3.4. Spirometer test profiles

Typical profiles obtained from SVC and MVV tests of spirometer are shown in Figs. 13 and 14. Fig. 13 shows the SVC profile of a subject under normal conditions. The graph along with the lung volume also shows the number of times inspiration and expiration occurred in a time frame of 1 min. The rise of the volume denotes intake of air i.e. breathing in while the decaying volume denotes the breathing out of air i.e. expiration.

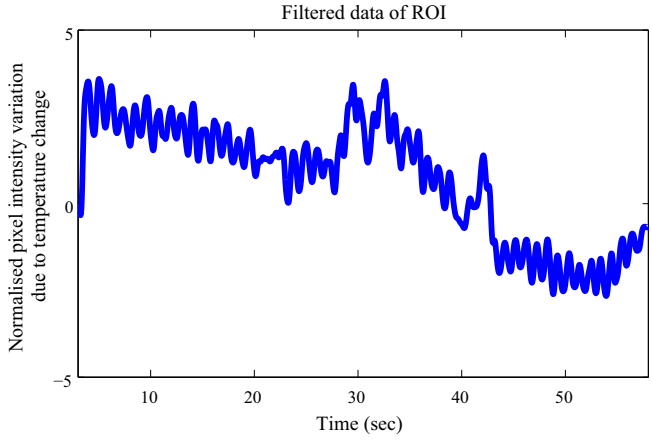

Fig. 11. Thermal profile obtained from ROI for hyperventilating condition.

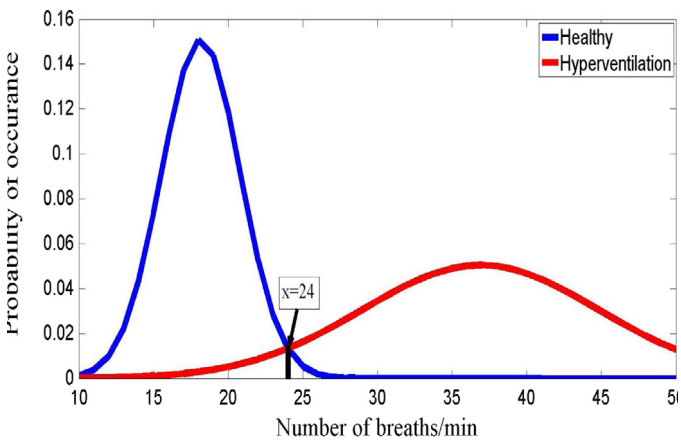

Fig. 12. Distributions for two classes and the decision boundary.

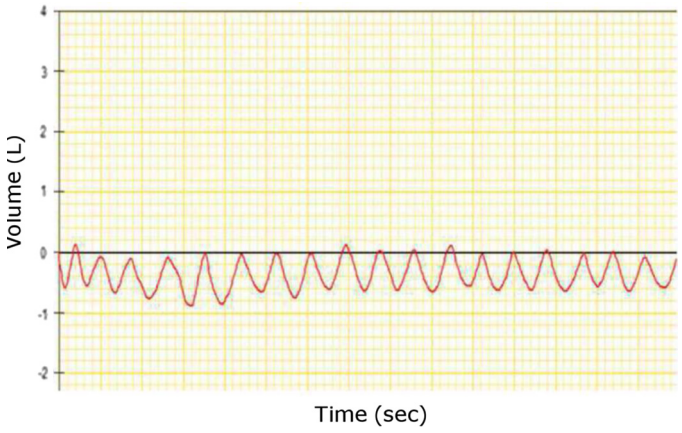

Fig. 13. Spirometer SVC profile while normal breathing condition.

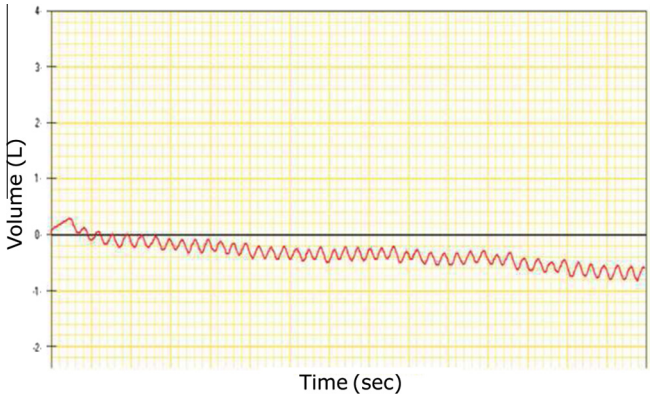

Fig. 14. Spirometer MVV profile obtained from ROI corresponding to hyperventilating condition.

For MVV similarly the subjects were asked to take very short and rapid breaths for about 1 min i.e. they were asked to artificially hyperventilate which gave the following profile. The figure shows the respiration profile which is found to be fast (almost 44 breaths/min as compared to 20 breaths/min under normal conditions) denoting hyperventilation syndrome. Spirometer profiles have been used to signify the erratic breath pattern during hyperventilation (Fig. 14).

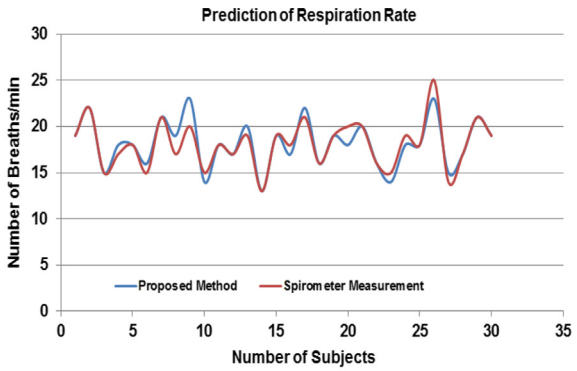

(a) Normal Breathing

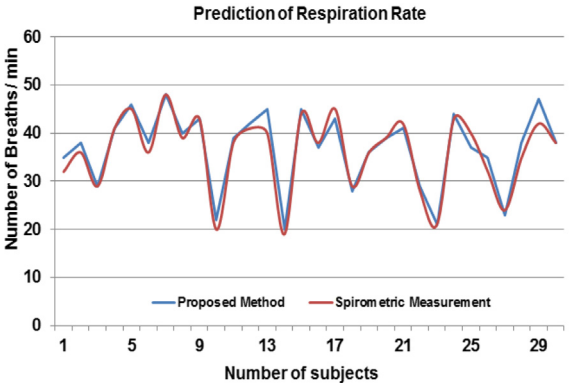

(b) Breathing during Hyperventilation

Fig. 15. Comparison of result with ground truth measurement.

3.5. Comparison

The techniques used in previous studies for detecting RR and its comparison with our proposed method are shown in Table 2.

The main advantage of this methodology lies in the fact that the algorithm allows for certain amount of head movements and the computation time is much less (only one to two mins.) than the other methodologies previously used.

A comparison of the estimated RR both during normal as well as hyperventilating condition using proposed method and spirometer measurement have been plotted as shown in Fig. 15. The predicted RR using proposed methodology is found to be highly correlated with the contact based measurement.

Table 2
Table showing the comparison of some reported works and our methodology for computing RR.

Reference	Main features	Comparison with our methodology
Al-khalidi et al. [42]	1. Warm eyes, cool nose 2. Narrow tracking range 3. Computationally slow	1. Initialized on the basis of cool and warm part 2. Nostril is tracked as ROI 3. Tracking on the basis of corner feature 4. Time efficient real time application
Chekmenev et al. [25]	1. Tracking or real time processing not done	1. Frame extraction not required as video processing is done
Zhu et al. [13]	1. Three tracking ROI and one measuring ROI 2. MSL tracking algorithm 3. Tracking with significant head movement but error when more than two tracking ROI is lost	1. One single ROI 2. Corner feature based robust algorithm causing no loss of the tracking ROI under significant head movement
Fei and Pavlidis [43]	1. CO_2 absorption band thermal images 2. Tracking of airflow 3. Fails in significant head movement	1. Simple thermal image is sufficient and no optical filter is needed 2. Significant head movement can be allowed
Alkali et al. [44]	1. Template matching of the face and manually selected ROI	1. Tracking of whole face is not required, only the ROI is tracked
Saatchi et al. [45]	1. Tracking of head curve in each frame for successful tracking in wide angle variation 2. Finding of coolest and warmest part in each frame	1. No need to track head 2. More accurate in head movement as tracking of direct ROI

4. Conclusion

The non-contact form of detection of hyperventilation using our proposed method may be more beneficial compared to the existing conventional methods like respiration belts and spirometer as it saves the person from the discomfort and panic associated with the contact based methods. The results have been further validated using spirometer and it has shown comparable accuracy. Our proposed technique can be arranged at any place wherever the patients feel themselves to be comfortable and completed in less computation time with reduced complexity. Furthermore this methodology can be implemented in smart phones and tablets for daily tracking and monitoring of hyperventilation and other breathing problems. However, the cost of thermal infrared cameras is the main limitation of this study. But with the growing interest of thermography and its application in various fields, it may be postulated that cost effective solutions will come in the near future.

Acknowledgment

The authors would like to thank the participants for their consent and co-operation in the experiment and also the technicians for their help in conducting the experiment.

References

[1] T.-Y. Cheng, C. Herman, Motion tracking in infrared imaging for quantitative medical diagnostic applications, Infrared Phys. Technol. 62 (2014) 70–80, http://dx.doi.org/10.1016/j.infrared.2013.10.009.
[2] B. Lahiri, S. Bagavathiappan, T. Jayakumar, J. Philip, Medical applications of infrared thermography: a review, Infrared Phys. Technol. 55 (4) (2012) 221–235, http://dx.doi.org/10.1016/j.infrared.2012.03.007.
[3] L.C. Lum, Hyperventilation and anxiety state, J. Roy. Soc. Med. 74 (1) (1981) 1–4.
[4] Hyperventilation: MedlinePlus Medical Encyclopedia. <http://www.nlm.nih.gov/medlineplus/ency/article/003071.htm>.
[5] S. Telles, S. Reddy, H. Nagendra, Oxygen consumption and respiration following two yoga relaxation techniques, Appl. Psychophysiol. Biofeedback 25 (4) (2000) 221–227.
[6] X. Bellei, K. Mestha, P. Graham, Monitoring Respiration with a Thermal Imaging System, US Patent 2012028985, 2012.
[7] R. Murthy, I. Pavlidis, Non-contact monitoring of breathing function using infrared imaging, IEEE Eng. Med. Biol. Mag. (8) (2005) 1–17.
[8] V.V. Mikhailov, Changes in respiration following voluntary hyperventilation, Bull. Exp. Biol. Med. 49 (6) (1960) 558–561, http://dx.doi.org/10.1007/BF00782104.
[9] L. Freeman, P. Nixon, Chest pain and the hyperventilation syndrome–some aetiological considerations, Postgrad. Med. J. 61 (721) (1985) 957–961.
[10] A.P. Davis, A.H. Lettington, Principle of thermal imaging, in: Application of Thermal Imaging, Taylor & Francis Group, 1988, pp. 275–286 (Chapter 8).
[11] M. Vollmer, K.-P. Möllmann, Infrared Thermal Imaging: Fundamentals, Research and Applications, vol. 32, John Wiley & Sons, 2010.
[12] Respiratory System. <http://users.rcn.com/jkimball.ma.ultranet/BiologyPages/P/Pulmonary.html>.
[13] Z. Zhu, J. Fei, I. Pavlidis, Tracking human breath in infrared imaging, 5th IEEE Symposium on Bioinformatics and Bioengineering, vol. 77204, 2005, pp. 227–231.
[14] Michael J. Zvolensky, Georg H. Eifert, A review of psychological factors/processes affecting anxious responding during voluntary hyperventilation and inhalations of carbon dioxide-enriched air, Clin. Psychol. Rev. 21 (3) (2001) 375–400, http://dx.doi.org/10.1016/S0272-7358(99)00053-7.
[15] A.E. Meuret, T. Ritz, F.H. Wilhelm, W.T. Roth, Voluntary hyperventilation in the treatment of panic disorder – functions of hyperventilation, their implications for breathing training, and recommendations for standardization, Clin. Psychol. Rev. 25 (3) (2005) 285–306, http://dx.doi.org/10.1016/j.cpr.2005.01.002.
[16] S.S. Kety, C.F. Schmidt, The effects of active and passive hyperventilation on cerebral blood flow, cerebral oxygen consumption, cardiac output, and blood pressure of normal young men 1, J. Clin. Investig. 25 (1) (1946) 107–119, http://dx.doi.org/10.1172/JCI101680.
[17] K. Chang, S. Barnes, E. Haacke, R. Grossman, Y. Ge, Imaging the effects of oxygen saturation changes in voluntary apnea and hyperventilation on susceptibility-weighted imaging, Am. J. Neuroradiol. 35 (6) (2014) 1091–1095.
[18] Clinical validation of the ECG-derived respiration (EDR) technique, Comput. Cardiol. 13 (1986) 507–510. <http://www.physionet.org/physiotools/edr/cic86/edr86.html>.
[19] J.A.M. Partinen, Detection of sleep apneas by the static charge-sensitive bed, in: Proc. 6th European Congress on Sleep Research, Zurich, 1982.
[20] B.H. Larson, Signal Processing Techniques for Non-invasive Monitoring of Respiration and Heart Rate Ph.D. thesis, University of Houstan, 1987.
[21] D. Barschdorff, W.Z.W. Zhang, Respiratory rhythm detection with photoplethysmographic methods, in: Proceedings of 16th Annual International Conference of the IEEE Engineering in Medicine and Biology Society, 1994, pp. 912–913, http://dx.doi.org/10.1109/IEMBS.1994.415209.
[22] K. Nepal, E. Biegeleisen, Apnea detection and respiration rate estimation through parametric modelling, in: Proceedings of the IEEE 28th Annual Northeast Bioengineering Conference (IEEE Cat. No. 02CH37342), IEEE, 2002, pp. 277–278, http://dx.doi.org/10.1109/NEBC.2002.999573.
[23] E.F. Greneker, Radar sensing of heartbeat and respiration at a distance with applications of the technology, Radar Sensor Technology II, vol. 449, 1997, pp. 150–154, http://dx.doi.org/10.1049/cp:19971650.
[24] I. Pavlidis, N.L. Eberhardt, J.A. Levine, Seeing through the face of deception, Nature 415 (6867) (2002) 35, http://dx.doi.org/10.1038/415035a.
[25] S.Y. Chekmenev, H. Rara, A.A. Farag, Non-contact, wavelet-based measurement of vital signs using thermal imaging, in: The First International Conference on Graphics, Vision and Image Processing, 2005, pp. 107–112.
[26] R. Murthy, I. Pavlidis, Noncontact measurement of breathing function, IEEE Eng. Med. Biol. 25 (3) (2006) 57–67.
[27] J. Fei, Z. Zhu, I. Pavlidis, Imaging breathing rate in the CO_2 absorption band, in: IEEE Engineering in Medicine and Biology 27th Annual Conference, 2005, pp. 700–705.
[28] M. Garbey, N. Sun, A. Merla, I. Pavlidis, Contact-free measurement of cardiac pulse based on the analysis of thermal imagery, IEEE Trans. Biomed. Eng. 54 (8) (2007) 1418–1426.
[29] J.N. Murthy, D. Absm, J.V. Jaarsveld, J. Fei, I. Pavlidis, R.I. Harrykissoon, J.F. Lucke, Thermal infrared imaging: a novel method to monitor airflow during polysomnography, Sleep 32 (11) (2009) 1521–1527.
[30] F. Al-khalidi, R. Saatchi, H. Elphick, D. Burke, F. Aces, An evaluation of thermal imaging based respiration rate monitoring in children department of engineering and mathematics, reader in computer engineering and digital signal processing, Sheffield Children s NHS Foundation Trust, Sheffield, UK, Am. J. Eng. Appl. Sci. 4 (4) (2011) 586–597.
[31] T. Matsui, S. Suzuki, K. Ujikawa, T. Usui, S. Gotoh, M. Sugamata, Z. Badarch, S. Abe, Development of a non-contact screening system for rapid medical inspection at a quarantine depot using a laser Doppler blood-flow meter, microwave radar and infrared thermography, J. Med. Eng. Technol. 33 (5) (2009) 403–409.
[32] Abbas K. Abbas, Konrad Heimann, Katrin Jergus, Thorsten Orlikowsky, Steffen Leonhardt, Neonatal non-contact respiratory monitoring based on real-time infrared thermography, Biomed. Eng. Online 10 (1) (2011) 93.
[33] Gregory F. Lewis, Rodolfo G. Gatto, Stephen W. Porges, A novel method for extracting respiration rate and relative tidal volume from infrared thermography, Psychophysiology 48 (7) (2011) 877–887.
[34] H. Tao, T.S. Huang, Visual estimation and compression of facial motion parameters elements of a 3D model-based video coding system, Int. J. Comput. Vis. 50 (2) (2002) 111–125.
[35] D. Duong, D. Shastri, P. Tsiamyrtzis, I. Pavlidis, Spatiotemporal reconstruction of the breathing function, Med. Image Comput. Comput.-Assisted Intervent. – MICCAI 2012 (2012) 149–156.
[36] J. Fei, I. Pavlidis, S. Member, Thermistor at a distance: unobtrusive measurement of breathing, IEEE Trans. Biomed. Eng. 57 (4) (2010) 988–998.
[37] Y. Zhou, P. Tsiamyrtzis, P. Lindner, I. Timofeyev, I. Pavlidis, Spatiotemporal smoothing as a basis for facial tissue tracking in thermal imaging, IEEE Trans. Biomed. Eng. 60 (5) (2013) 1280–1289.
[38] I. Pavlidis, Tracking human breath in infrared imaging, in: Fifth IEEE Symposium on Bioinformatics and Bioengineering (BIBE'05), IEEE, 2005, pp. 227–231, http://dx.doi.org/10.1109/BIBE.2005.55.
[39] C. Shi, Jianbo Tomasi, Good features to track, in: IEEE Computer Society Conference on Computer Vision and Pattern Recognition, 1994, Proceedings CVPR '94, 1994, 1994, pp. 593–600.
[40] C. Harris, M. Stephens, A combined corner and edge detector, in: Proceedings of the Alvey Vision Conference 1988, Alvey Vision Club, 1988, pp. 147–151, http://dx.doi.org/10.5244/C.2.23.
[41] B.D. Lucas, An iterative image registration technique with an application to stereo vision, in: Proceedings 7th International Joint Conference on Artificial Intelligence, 1981, pp. 674–679.
[42] F.Q. Al-khalidi, R. Saatchi, D. Burke, H. Elphick, Tracking human face features in thermal images for respiration monitoring, in: 2010 ACS/IEEE International Conference on Computer Systems and Applications, AICCSA 2010, 2010, pp. 1–6.
[43] J. Fei, I. Pavlidis, Analysis of breathing air flow patterns in thermal imaging, in: Proceedings of the 28th IEEE EMBS Annual International Conference, 2006, pp. 946–952.
[44] A.H. Alkali, R. Saatchi, H. Elphick, D. Burke, Facial tracking in thermal images for real-time noncontact respiration rate monitoring, in: 2013 European Modelling Symposium, Ieee, 2013, pp. 265–270, http://dx.doi.org/10.1109/EMS.2013.46.
[45] F.Q. Al-Khalidi, R. Saatchi, D. Burke, H. Elphick, Facial tracking method for noncontact respiration rate monitoring, in: 7th International Symposium on Communication Systems Networks and Digital Signal Processing (CSNDSP) 2010, 2010, pp. 751–754.